Generating Greenberger-Horne-Zeilinger states with squeezing and postselection

Byron Alexander[1,*] John J. Bollinger[2,†] and Hermann Uys[1,3,‡]
[1]*Department of Physics, Stellenbosch University, Stellenbosch Central 7600, Stellenbosch, South Africa*
[2]*National Institute of Standards and Technology, Boulder, Colorado 80305, USA*
[3]*Council for Scientific and Industrial Research, National Laser Centre, Brummeria, Pretoria 0184, South Africa*

(Received 9 December 2019; revised manuscript received 23 April 2020; accepted 7 May 2020; published 1 June 2020)

Many quantum state preparation methods rely on a combination of dissipative quantum state initialization followed by unitary evolution to a desired target state. Here we demonstrate the usefulness of quantum measurement as an additional tool for quantum state preparation. Starting from a pure separable multipartite state, a control sequence, which includes rotation, spin squeezing via one-axis twisting, quantum measurement, and postselection, generates highly entangled multipartite states, which we refer to as *projected squeezed* (PS) states. Through an optimization method, we then identify parameters required to maximize the overlap fidelity of the PS states with the maximally entangled Greenberger-Horne-Zeilinger (GHZ) states. The method leads to an appreciable decrease in the state preparation time of GHZ states for successfully postselected outcomes when compared to preparation through unitary evolution with one-axis twisting only.

DOI: 10.1103/PhysRevA.101.062303

I. INTRODUCTION

The emerging technologies of quantum computing, quantum communication, and quantum sensing rely principally on quantum phenomena such as superposition and entanglement for their unique capabilities. These phenomena allow quantum computational devices to overcome limits set by their classical counterparts in the computational speed of complex algorithms. Furthermore, quantum sensors [1], i.e., devices which utilize quantum correlations to improve measurement sensitivity by suppressing phase noise in multiparticle interferometry [2–4], demonstrate the potential of quantum-enhanced technology. Examples include enhanced performance in atomic clocks [5,6], magnetic field detection [7], and precision of frequency measurements [8,9].

To this end, it becomes paramount to develop well-defined and efficient protocols to produce and further exercise control over states of quantum bits that exhibit desired quantum mechanical traits. Our investigation focuses on establishing a protocol that uses quantum control operations combined with measurement and postselection to produce highly entangled metrologically relevant states. We will refer to these states as *projected squeezed* (PS) states. We further study optimization of the control parameters that produce maximal overlap of the projected squeezed state with the well-known *Greenberger-Horne-Zeilinger* (GHZ) state (commonly referred to as the maximally entangled state or GHZ state; see [10–14]). For a multipartite system consisting of N qubits, the GHZ state reads as follows:

$$|GHZ\rangle := \frac{|0\rangle^{\otimes N} + |1\rangle^{\otimes N}}{\sqrt{2}}. \tag{1}$$

Due to their high level of entanglement, the GHZ states are of importance in various applications such as metrology [11], quantum teleportation [15], quantum computing [16], and quantum secret sharing [17]. There are numerous proposed schemes for producing GHZ states, particularly in the context of cavity quantum electrodynamics [18–23]. Some of the most successful implementations have been in trapped-ion systems, where 14-ion GHZ states [24] and more complex entangled states of up to 20 ions [25] have been observed. Recently, 20-qubit GHZ states have been generated through unitary evolution with Rydberg atom qubits [26] and superconducting circuit qubits [27]. Using postselection in a linear optical system, GHZ states of 10 photons have been reported [28]. More recently, 12-photon entanglement [29] and 18-qubit hyperentanglement [30] have been demonstrated. Closely related to the photon GHZ states are the so-called NOON states, which also exhibit an improvement on the standard quantum limit with regard to phase-error measurements [31]. A number of proposed schemes for producing NOON states exist [32–35].

Our approach expands the typical suite of quantum state preparation tools, which relies on dissipative state initialization followed by unitary evolution, to include quantum measurement. Examples of measurement-based state preparation include spin-squeezed states [36,37] and other highly entangled states [38–43]. The particular example discussed here illustrates that nontrivial speed-up can be achieved as compared to state preparation with unitary evolution only. This speed-up occurs for all successfully postselected measurements, even though it might come at the cost of increased overall preparation time due to the statistical nature of the

*alxbyr001@myuct.ac.za
†john.bollinger@nist.gov
‡hermann.uys@gmail.com

postselection process. Nonetheless, this aspect may be of interest to beat decoherence timescales in appropriate scenarios.

The setup we have in mind is an ensemble of two-level systems, with eigenstates represented in the collective pseudospin basis (also known as the *Dicke state basis* [44]). The projected squeezed state is produced through a sequence of control operations including initialization, rotation, spin squeezing [45], quantum measurement, and postselection. Experimentally, the main technical challenge is carrying out a projective measurement of the collective spin projection quantum number (as opposed to a measurement in the single-particle basis), as all other aspects are well established.

The one-axis twisting spin-squeezing operator (also known as the *Kitagawa shearing gate*), which was introduced in a seminal paper [45], is described by the following unitary transformation:

$$\hat{U}_{Sq}(t) = \exp\big(-i\chi t\hat{J}_z^2\big). \tag{2}$$

One-axis twisting has been realized with trapped ions [46], neutral atoms [47,48], and superconducting circuits [27]. Here, χ quantifies the strength of the squeezing interaction, and

$$\hat{J}_k := \sum_i^N \frac{1}{2}\sigma_i^k, \tag{3}$$

where $k = x, y, z$ and σ_i^k is the k component of the usual Pauli spin operator for the ith two-level system in an ensemble of N systems. This definition preserves the spin commutation relation $[\hat{J}_x, \hat{J}_y] = 2i\epsilon_{xyz}\hat{J}_z$ for the pseudospin $\hat{J}^2 = \hat{J}_x^2 + \hat{J}_y^2 + \hat{J}_z^2$. In what follows, we will restrict ourselves to a subspace of the full pseudospin Hilbert space, namely, the fully symmetric (Dicke) eigenstates for which

$$\hat{J}_z\left|\frac{N}{2}, \frac{N}{2} - m\right\rangle = \left(\frac{N}{2} - m\right)\left|\frac{N}{2}, \frac{N}{2} - m\right\rangle,$$

with $m = 0, 1, 2, \ldots, N$, and

$$\hat{J}^2\left|\frac{N}{2}, \frac{N}{2} - m\right\rangle = \left(\frac{N}{2}\right)\left(\frac{N}{2} + 1\right)\left|\frac{N}{2}, \frac{N}{2} - m\right\rangle.$$

A method for constructing the Dicke states from the single spin basis is discussed in [46].

II. METHOD

We now describe the steps in the state preparation protocol. As an initial state, we choose the pure, separable state

$$|\psi(0)\rangle = \left|\frac{N}{2}, \frac{N}{2}\right\rangle. \tag{4}$$

The protocol, in sequence, consists of the following operations:

Step 1. An initial rotation by $\frac{\pi}{2}$ about the x axis to form what is known as the *coherent spin* (CS) state,

$$|CS\rangle = \frac{1}{2^{N/2}}\sum_{M=-\frac{N}{2}}^{\frac{N}{2}}\binom{N}{\frac{N}{2}+M}^{1/2}\left|\frac{N}{2}, M\right\rangle. \tag{5}$$

We can visually represent any state $|\psi\rangle$ on the Bloch sphere by considering the modulus squared of the projection of that state onto a rotated coherent spin state, $H = |\langle\psi|\exp(-i\phi\hat{J}_z)\exp(-i\theta\hat{J}_x)|CS\rangle|^2$, where θ and ϕ are, respectively, the polar and azimuthal angles. These are commonly referred to as *Husimi plots* [49]. This projection, when $|\psi\rangle = |CS\rangle$, is shown on a unit sphere in Fig. 1(a). It shows that the rms width of H is uniform in all directions for this case.

Step 2. The coherent spin state then undergoes *squeezing* by the unitary transformation given by Eq. (2), where the magnitude of squeezing is controlled by choices of the squeezing parameter χt [46]. This is shown in Figs. 1(b) and 1(c) for different values of χt. As we can see, when acting on a coherent spin state, the squeezing operator reduces the spin uncertainty along one spin axis at the expense of increasing the uncertainty along an orthogonal spin axis. The uncertainty is stretched symmetrically about an axis tilted slightly with respect to the x axis, as opposed to the x axis itself [see Figs. 1(b) and 1(c)]. This is known as the *antisqueezing axis*. To maximize the overlap fidelity with the GHZ state, it is necessary, for low squeezing values ($\chi t \lesssim 0.25$), to rotate about the y axis such that the antisqueezed axis is aligned with the x axis (the magnitude of rotation can be determined empirically, by maximizing the probability distribution on the equatorial plane, or analytically; see Eq. (3) of [45]). Note that no rotation is required for larger squeezing values of $\chi t = 0.4$ (or $\pi/4$), since for these values the antisqueezed axis is already aligned with the x axis.

A choice of the squeezing parameter of approximately $\chi t = 0.25$ starts producing a projection sufficiently flat so as to create a probability ring that wraps around the sphere [as shown in Fig. 1(c)].

Step 3. Following the squeezing, we rotate about the x axis until the ring is aligned with the z axis, as shown in Fig. 2.

Step 4. The appropriate quantum measurement is carried out and the desired state is postselected based on the measurement outcome. The Kraus operators that describe our quantum measurement are chosen as follows:

$$A_C := \sum_M \sqrt{\Pr(M|C)}\left|\frac{N}{2}, M\right\rangle\left\langle\frac{N}{2}, M\right|, \tag{6}$$

with *Gaussian probability distribution*

$$\Pr(M|C) := \frac{1}{\sqrt{2\pi\sigma^2}}\exp\left[-\frac{(M-C)^2}{2\sigma^2}\right]. \tag{7}$$

As required, the operators A_C obey the normalization condition $\int A_C A_C^\dagger dC = I$. Physically, a measurement of $A_{C'}$, with outcome C', will project an initial wave function onto a superposition of states $|\frac{N}{2}, M\rangle$ with amplitudes following a Gaussian distribution and centered on C', with width σ.

Since the set of allowed measurement outcomes $\{C\}_{C\in\mathbb{R}}$ is continuous, the resultant quantum state after measurement is thus given by

$$\rho \mapsto \tilde{\rho}_{\text{final}} = \frac{A_C\rho A_C^\dagger dC}{\text{Tr}[A_C\rho A_C^\dagger dC]}, \tag{8}$$

where ρ denotes the density matrix that describes the state of our system, and $\text{Tr}[A_C\rho A_C^\dagger dC]$ is the probability density to observe a measurement outcome in the interval $[C, C + dC]$

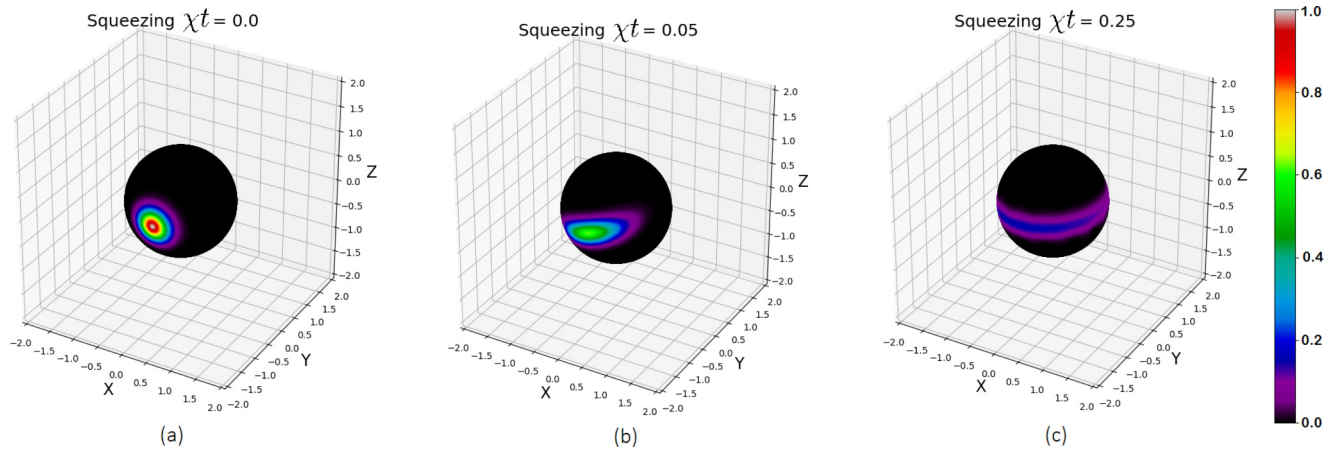

FIG. 1. Husimi plot of the CS state after varied squeezing ($N = 50$).

(see [50]). For computational purposes, we have to discretize the distribution $\Pr(M|C)$ by binning the C axis and integrating over each bin to obtain probabilities instead of probability densities, thus allowing us to model the measurement statistics numerically.

To generate the desired state, the quantum measurement defined by Eq. (6) is executed, and only outcomes with $C \approx 0$ are postselected. This produces what we refer to as a *projected squeezed* state, henceforth denoted $|PS\rangle$. The resultant state after measurement, as shown in Fig. 3, consists of two probability lobes concentrated on opposing sides of the Bloch sphere. Here we used $N = 50$, $\chi t = 0.4$ and measurement operator variance $\sigma^2 = 22$ for optimization reasons which will be discussed shortly.

Step 5. Finally, we generate a state which closely resembles the GHZ state by executing a rotation by $\frac{\pi}{2}$ about the y axis. Then, the resemblance to the GHZ state is quantified by computing the measure of the "closeness" of two pure quantum states: $\mathcal{F} = |\langle PS|GHZ\rangle|^2$, where $|GHZ\rangle$ is defined by Eq. (1). $\mathcal{F}$ is known as the *overlap fidelity*.

For completeness, we plot in Fig. 4 the modulus squared of the probability distribution of the PS state in the Dicke basis as generated in step 4 of the protocol, and after the rotation about the y axis in step 5. It shows that any imperfect overlap is due to the unintended occupation of close-lying states other than $|\frac{N}{2}, \pm\frac{N}{2}\rangle$ with small probability amplitudes.

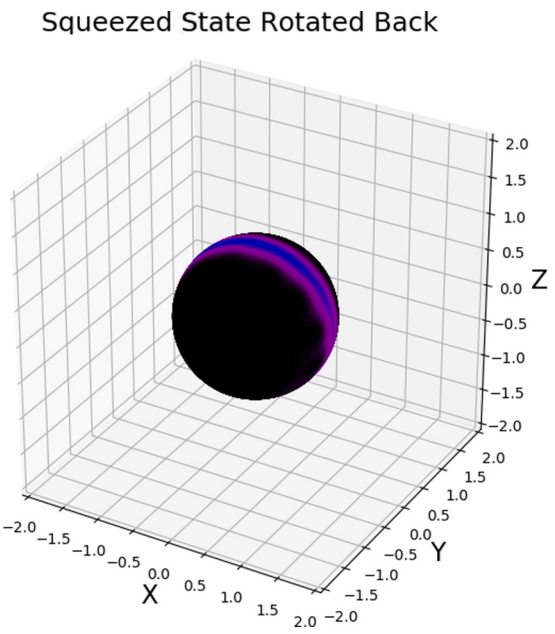

FIG. 2. Husimi plot of the spin state at step 3 of the protocol.

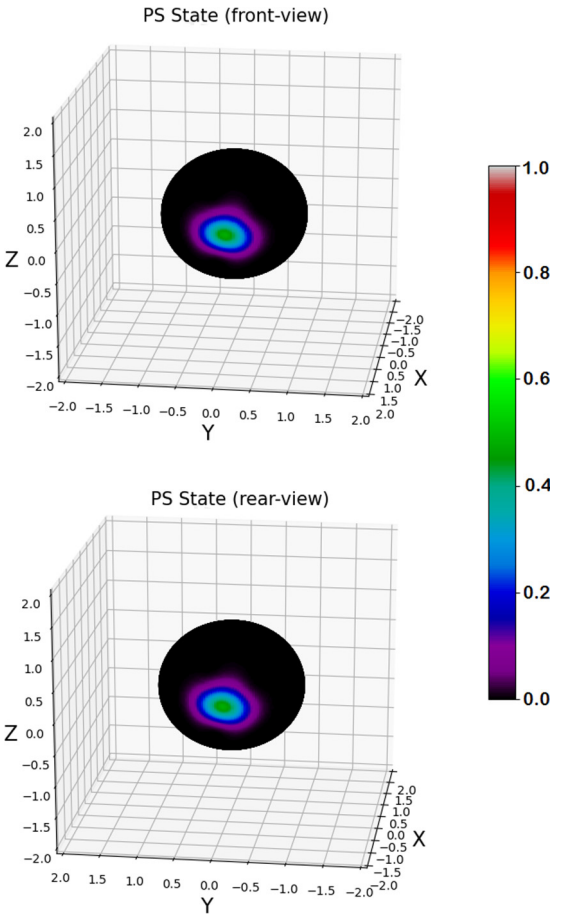

FIG. 3. Husimi plot of projected spin state (step 4).

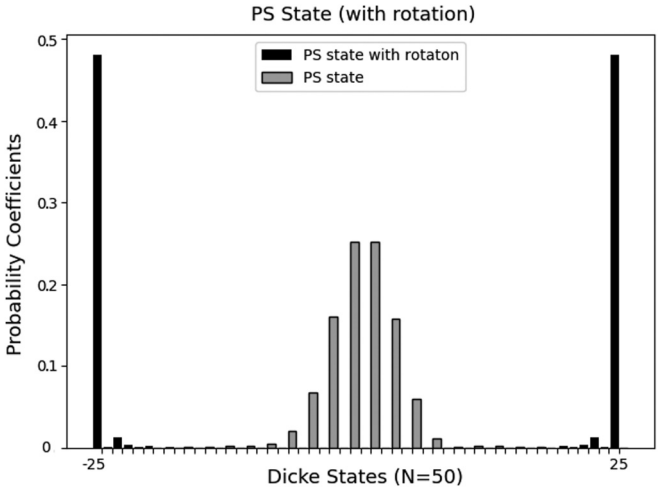

FIG. 4. Probability coefficients of the *PS* state in a Dicke state basis.

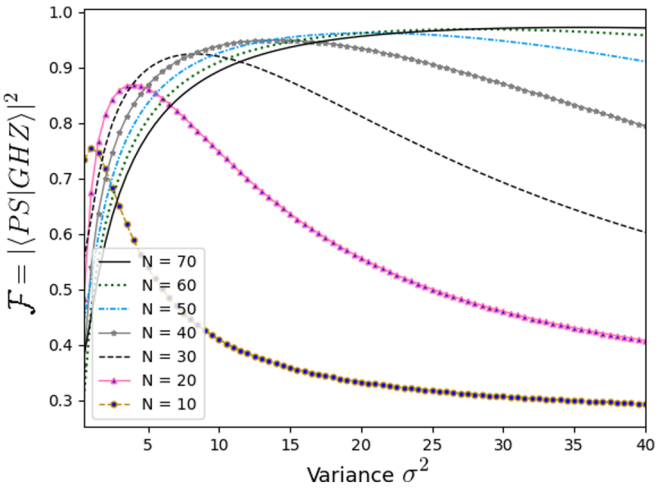

FIG. 6. Overlap fidelity of PS and GHZ states as a function of σ^2, for varied N ($\chi t = 0.40$).

III. OPTIMIZATION

A numerical optimization method (random walk–Markov chain Monte Carlo (MCMC)-type regime; see [51,52]) is now employed to find parameters of σ^2 and χt that maximize the overlap fidelity with the GHZ state.

Given initial values of σ^2 (the variance used in defining the measurement operators) and χt (the squeezing parameter), we define an initial vector $(\sigma_0^2, \chi t_0)$. The numerical algorithm stochastically traverses the parameter space in steps $(d\sigma^2, d\chi t)$ by evaluating the vector

$$(\sigma_1^2, \chi t_1) := (\sigma_0^2, \chi t_0) + (d\sigma^2, d\chi t)$$

for each iteration. The increments $d\sigma^2$ and $d\chi t$ are random variables in that they are respectively chosen from Gaussian probability distributions centered at zero (with the variance of these Gaussian distributions appropriately chosen to minimize the time of computation). For iteration n, the overlap fidelity is computed for parameter values $(\sigma_n^2, \chi t_n)$. If the fidelity is increased, the new vector is retained; otherwise, we reject the step and retain the previous vector $(\sigma_{n-1}^2, \chi t_{n-1})$. Subsequently, we compute a new vector and again compare this to the previous one. This process is continued until we identify parameters which produce an overlap fidelity value that is greater than or equal to a fixed threshold value. With $N = 50$, this optimization leads to a maximum of $\mathcal{F} \approx 0.97$ for the parameters $\chi t \approx 0.40$ and $\sigma^2 = 22$.

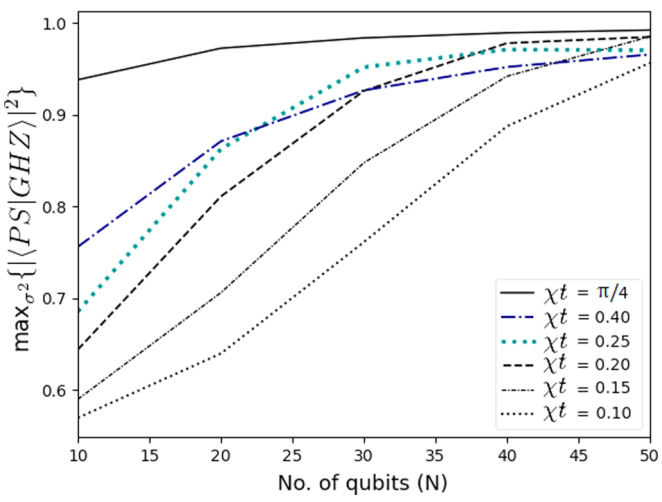

FIG. 5. Maximal GHZ overlap fidelity for varied squeezing times.

IV. ANALYSIS AND EFFICIENCY

To map out cross sections of the optimization landscape, we fixed individual parameters (after they have been optimized) while allowing the others to vary. This first shows that the maximum fidelity monotonically increases with increasing particle number N, as illustrated in Fig. 5, for different values of χt.

In Fig. 6, χt is fixed at 0.40 and the fidelity is plotted as a function of σ^2 for different particle numbers. It confirms that the maximum fidelity increases with N and shows that at larger particle number, the protocol is much less sensitive to variations in σ, producing high fidelity over wider regions of the variance. Figure 7 shows the fidelity as a function of variance for fixed $N = 50$ and for different values of the squeezing χt. There is no clear monotonic relationship between $\mathcal{F}$ and χt, but rather we attain local maxima in $\mathcal{F}$ values for $\chi t \in \{0.10, 0.15, 0.20, 0.25, 0.40, \pi/4\}$.

It is important to note that an exact GHZ state can be produced (with $\mathcal{F} = 1$) by using only the squeezing interaction with $\chi t = \frac{\pi}{2}$ and a rotation.[1] We emphasize that given $\chi t \approx 0.25$ (or 0.40), our measurement-based protocol produces highly entangled GHZ-type states about a factor 6 (or, respectively, a factor 4) faster than the coherent protocol with

[1]In principle, the PS state protocol could be employed to produce a state with $\mathcal{F} \to 1$ as $\sigma^2 \to \infty$ (for $\chi t = \frac{\pi}{2}$). This is clear since as the variance $\sigma^2 \to \infty$, the Gaussian distribution (7), which defines our Kraus measurement operators, tends to a uniform probability distribution and therefore the measurement operator, for $C' = 0$, approaches the identity.

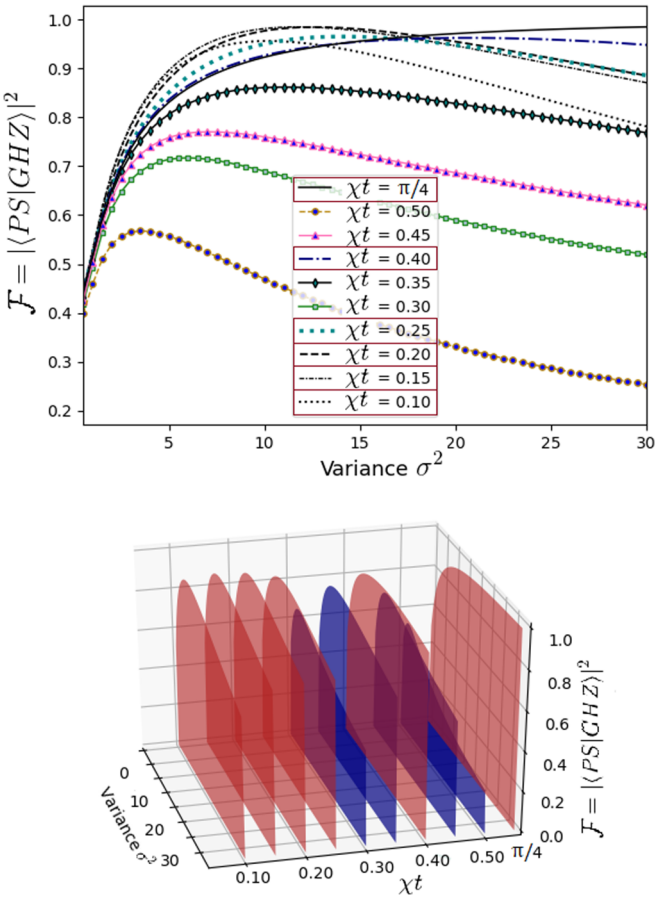

FIG. 7. Overlap fidelity of PS and GHZ states as a function of σ^2, for varied squeezing times ($N = 50$). For clarity, we show two perspectives of the data. Top: $\mathcal{F}$ is plotted for various χt on the same axes as indicated by the legend. Bottom: The same data as in the top panel in a 3D plot shows that the increase in maximum fidelity is not a monotonic function of χt. Curves outlined in red have local maxima in fidelity as a function of χt.

$\chi t = \frac{\pi}{2}$. As such, this measurement-based protocol may be preferable when the relevant decoherence timescale is close

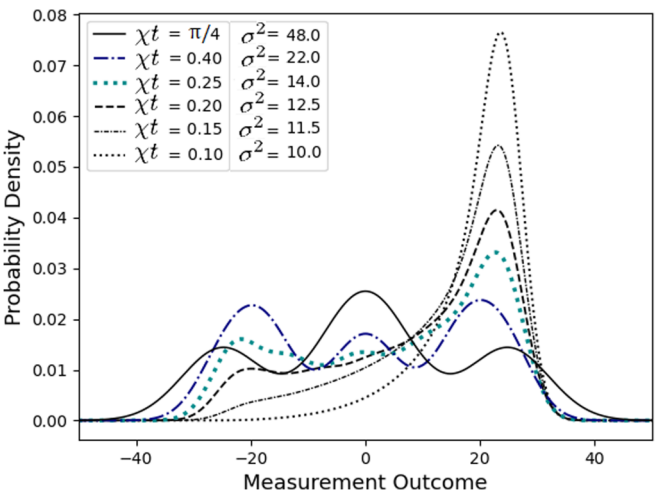

FIG. 8. Probability density distribution of measurement outcomes, C, for varied squeezing times ($N = 50$).

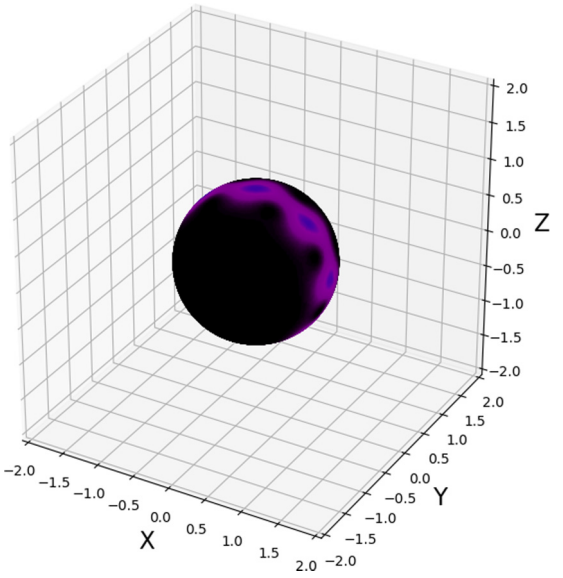

FIG. 9. Husimi plot of premeasurement squeezed state ($\chi t \approx 0.40$) rotated back about the x axis.

to $\chi t = \frac{\pi}{2}$ and as long as the increase in total time (including state preparation time and multiple attempts to guarantee a successful postselection) can be tolerated.

Over and above high overlap fidelity, an important consideration is the efficiency with which the PS state is produced. We will characterize a state preparation protocol as *efficient* if it requires low squeezing parameter χt (hence, less time required for squeezing), produces high overlap fidelity GHZ, and, given the inherent stochastic nature of the process, has a high measurement outcome probability.

Using the MCMC optimization protocol, we find that maxima in the overlap fidelity between the PS and GHZ states (varying N and σ^2) occur for low squeezing values $\chi t \in [0.10, 0.25]$ and for specific higher squeezing values

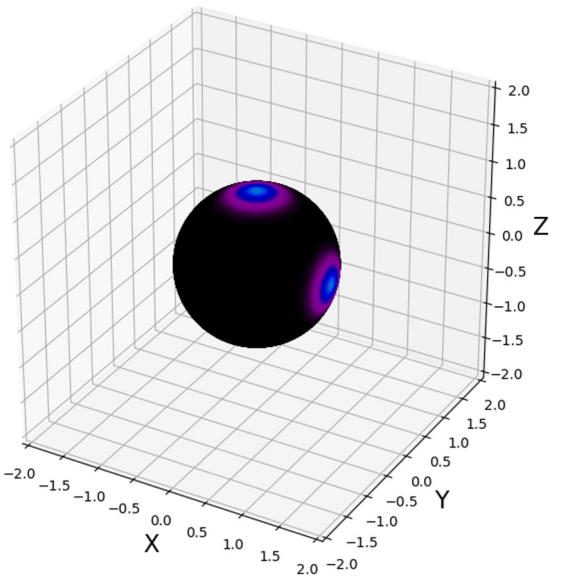

FIG. 10. Husimi plot of premeasurement squeezed state ($\chi t \approx \pi/4$) rotated back about the x axis.

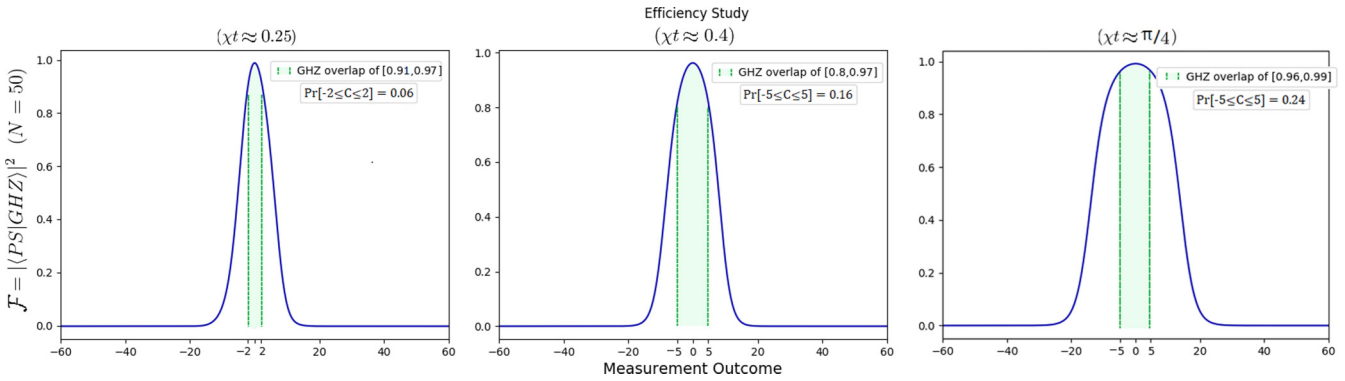

FIG. 11. Selected plots of $\mathcal{F}$ as a function of the measured outcome C. The vertical green lines indicate the range of outcomes C that yield $\mathcal{F}$ values falling in the range $[\cdot, \cdot]$ indicated in the text box in each subfigure. The total likelihood $\Pr[\cdot]$ of observing one of those outcomes is also indicated.

$\chi t \in \{0.40, \frac{\pi}{4}\}$ ($\chi t = \frac{\pi}{2}$, as stated above, requires no measurement). We plot in Fig. 8 the probability density for obtaining measurement outcomes $\{C\}_{C\in[-50,50]}$ for the aforementioned squeezing times. For comparison, the full premeasurement Husimi plots are shown in Figs. 2, 9, and 10 ($\chi t \in \{0.25, 0.40, \frac{\pi}{4}\}$).

There are distinct probability peaks in each of the probability distributions represented in Fig. 8. These peaks are due to the probability lobes seen in the Husimi plots of the rotated squeezed state. The maxima of the central peaks correspond to our desired postselected outcome $C' = 0$. Figure 11 plots the overlap fidelity $\mathcal{F}$ for select local maxima squeezing

TABLE I. The range (co-domain) $\mathscr{R}(\cdot)$ of the overlap fidelity $\mathcal{F}$ taken over some chosen interval $C \in [\cdot, \cdot]$ of measurement outcomes and the respective probability $\Pr[\cdot]$ of obtaining outcomes in this interval. For $\chi t = \pi/4$, we show results for $[-10, 10]$, $[-5, 5]$, and $[-2, 2]$ measurement outcome intervals as the range of GHZ overlap fidelity for the $[-2, 2]$ interval is already of the order of 10^{-3}.

$\chi t \approx 0.10$, $N = 50$, $\sigma^2 = 10$.					
$\mathscr{R}(\mathcal{F})_{C\in[-5,5]}$	$\Pr[-5 \leqslant C \leqslant 5]$	$\mathscr{R}(\mathcal{F})_{C\in[-2,2]}$	$\Pr[-2 \leqslant C \leqslant 2]$	$\mathscr{R}(\mathcal{F})_{C\in[-1,1]}$	$\Pr[-1 \leqslant C \leqslant 1]$
$[0.43, 0.99]$	0.048	$[0.79, 0.99]$	0.019	$[0.89, 0.99]$	0.01
$\chi t \approx 0.15$, $N = 50$, $\sigma^2 = 11.5$					
$\mathscr{R}(\mathcal{F})_{C\in[-5,5]}$	$\Pr[-5 \leqslant C \leqslant 5]$	$\mathscr{R}(\mathcal{F})_{C\in[-2,2]}$	$\Pr[-2 \leqslant C \leqslant 2]$	$\mathscr{R}(\mathcal{F})_{C\in[-1,1]}$	$\Pr[-1 \leqslant C \leqslant 1]$
$[0.51, 0.99]$	0.107	$[0.86, 0.99]$	0.043	$[0.94, 0.99]$	0.022
$\chi t \approx 0.20$, $N = 50$, $\sigma^2 = 12.5$					
$\mathscr{R}(\mathcal{F})_{C\in[-5,5]}$	$\Pr[-5 \leqslant C \leqslant 5]$	$\mathscr{R}(\mathcal{F})_{C\in[-2,2]}$	$\Pr[-2 \leqslant C \leqslant 2]$	$\mathscr{R}(\mathcal{F})_{C\in[-1,1]}$	$\Pr[-1 \leqslant C \leqslant 1]$
$[0.56, 0.99]$	0.126	$[0.88, 0.99]$	0.051	$[0.95, 0.99]$	0.026
$\chi t \approx 0.25$, $N = 50$, $\sigma^2 = 14$.					
$\mathscr{R}(\mathcal{F})_{C\in[-5,5]}$	$\Pr[-5 \leqslant C \leqslant 5]$	$\mathscr{R}(\mathcal{F})_{C\in[-2,2]}$	$\Pr[-2 \leqslant C \leqslant 2]$	$\mathscr{R}(\mathcal{F})_{C\in[-1,1]}$	$\Pr[-1 \leqslant C \leqslant 1]$
$[0.59, 0.97]$	0.132	$[0.91, 0.97]$	0.055	$[0.95, 0.97]$	0.028
$\chi t \approx 0.40$, $N = 50$, $\sigma^2 = 22$.					
$\mathscr{R}(\mathcal{F})_{C\in[-5,5]}$	$\Pr[-5 \leqslant C \leqslant 5]$	$\mathscr{R}(\mathcal{F})_{C\in[-2,2]}$	$\Pr[-2 \leqslant C \leqslant 2]$	$\mathscr{R}(\mathcal{F})_{C\in[-1,1]}$	$\Pr[-1 \leqslant C \leqslant 1]$
$[0.80, 0.97]$	0.161	$[0.94, 0.97]$	0.067	$[0.96, 0.97]$	0.035
$\chi t \approx \pi/4$, $N = 50$, $\sigma^2 = 48$.					
$\mathscr{R}(\mathcal{F})_{C\in[-10,10]}$	$\Pr[-10 \leqslant C \leqslant 10]$	$\mathscr{R}(\mathcal{F})_{C\in[-5,5]}$	$\Pr[-5 \leqslant C \leqslant 5]$	$\mathscr{R}(\mathcal{F})_{C\in[-2,2]}$	$\Pr[-2 \leqslant C \leqslant 2]$
$[0.80, 0.99]$	0.409	$[0.96, 0.99]$	0.242	$[0.987, 0.992]$	0.104

parameters and highlights the resultant fidelity (for specific measurement outcome intervals). It shows that for $\chi t \approx 0.40$, measurement outcomes in the range $[-5, 5]$ have overlap fidelities in the range [0.80, 0.97]. The probability of obtaining a measurement result in this range is 0.16 (approximately one success for every six trials). There is therefore a very reasonable success ratio for projecting on states with at least moderately high overlap with the GHZ state.

Squeezing parameters $\chi t \approx 0.25$, 0.40 and $\pi/4$, respectively, yield maximal PS and GHZ state fidelity values (given a measurement outcome $C' = 0$) of 0.97, 0.97, and 0.99. A salient feature of squeezing $\chi t \approx \pi/4$, as compared to $\chi t \approx 0.25$ or 0.40, is that the desired postselected measurement outcome $C' = 0$ is the most probable outcome (see Fig. 8).

Efficiency results

In Table I, we summarize the efficiency of the protocol by showing the range (codomain) of $\mathcal{F}$ for particular measurement outcome intervals. The analysis presents results for the optimized set of squeezing parameters (with σ^2 chosen accordingly).

V. DISCUSSION

Using the method presented, one can create GHZ states with high fidelity in quantum spin systems. In trapped ion and neutral atom systems, state detection conventionally relies on fluorescence scattering from a dipole-allowed closed-cycle transition. This, however, projects the spins in the single-particle basis rather than the Dicke basis, which makes it an unsuitable quantum measurement for our purposes. In trapped-ion systems, one potential method for executing the collective measurement is to do state-dependent excitation of the ion motion using the optical dipole force [3]. The image current induced in the ion trap electrodes is expected to be proportional to the projection quantum number M and not to the individual ion state. This can be used to implement the measurement operator in Eq. (6).

Starting with the pure separable state $|\psi\rangle = |\frac{N}{2}, \frac{N}{2}\rangle$, we showed that by using a combination of spin squeezing, quantum measurement, and postselection, it is possible to generate many-particle GHZ states with high fidelity ($\mathcal{F} > 0.99$). It is a comparatively efficient method in the sense that despite its stochastic nature, we produce these highly entangled PS states for squeezing parameter χt that are significantly lower than that required when doing coherent squeezing [Eq. (2)] only. This may be beneficial for beating decoherence limitations in some experiments.

ACKNOWLEDGMENTS

We thank E. Jordan and R. Lewis-Swan for useful comments and discussions and I. Cirac for bringing this problem to our attention. We are also grateful to Sulona Kandhai, from the University of Cape Town, for fruitful discussions on employing numerical optimization methods. This project was funded by the CSIR and Department of Science and Technology.

[1] C. L. Degen, F. Reinhard, and P. Cappellaro, Quantum sensing, Rev. Mod. Phys. **89**, 035002 (2017).
[2] V. Giovannetti, S. Lloyd, and L. Maccone, Advances in quantum metrology, Nat. Photon. **5**, 222 (2011).
[3] O. Hosten, N. J. Engelsen, R. Krishnakumar, and M. A. Kasevich, Measurement noise 100 times lower than the quantum-projection limit using entangled atoms, Nature (London) **529**, 505 (2016).
[4] C. Gross, Spin squeezing, entanglement and quantum metrology with Bose-Einstein condensates, J. Phys. B: At. Mol. Opt. Phys. **45**, 103001 (2012).
[5] E. M. Kessler, P. Komar, M. Bishof, L. Jiang, A. S. Sørensen, J. Ye, and M. D. Lukin, Heisenberg-Limited Atom Clocks Based on Entangled Qubits, Phys. Rev. Lett. **112**, 190403 (2014).
[6] P. Komar, E. M. Kessler, M. Bishof, L. Jiang, A. S. Sørensen, J. Ye, and M. D. Lukin, A quantum network of clocks, Nat. Phys. **10**, 582 (2014).
[7] T. Ruster, H. Kaufmann, M. A. Luda, V. Kaushal, C. T. Schmiegelow, F. Schmidt-Kaler, and U. G. Poschinger, Entanglement-Based dc Magnetometry with Separated Ions, Phys. Rev. X **7**, 031050 (2017).
[8] S. F. Huelga, C. Macchiavello, T. Pellizzari, A. K. Ekert, M. B. Plenio, and J. I. Cirac, Improvement of Frequency Standards with Quantum Entanglement, Phys. Rev. Lett. **79**, 3865 (1997).
[9] F. Martin Ciurana, G. Colangelo, L. Slodička, R. J. Sewell, and M. W. Mitchell, Entanglement-Enhanced Radio-Frequency Field Detection and Waveform Sensing, Phys. Rev. Lett. **119**, 043603 (2017).
[10] M. Walter, D. Gross, and J. Eisert, Multi-partite entanglement, in *Quantum Information: From Foundations to Quantum Technology Applications* (Wiley Online Library, 2016), pp. 293–330.
[11] G. Tóth and I. Apellaniz, Quantum metrology from a quantum information science perspective, J. Phys. A: Math. Theor. **47**, 424006 (2014).
[12] V. Coffman, J. Kundu, and W. K. Wootters, Distributed entanglement, Phys. Rev. A **61**, 052306 (2000).
[13] D. A. Meyer and N. R. Wallach, Global entanglement in multiparticle systems, J. Math. Phys. **43**, 4273 (2002).
[14] D. M. Greenberger, M. A. Horne, and A. Zeilinger, Going beyond Bell's theorem, in *Bell's Theorem, Quantum Theory and Conceptions of the Universe* (Springer, Dordrecht, 1989), pp. 69–72.
[15] V. Gorbachev and A. Trubilko, Quantum teleportation of an Einstein-Podolsy-Rosen pair using an entangled three-particle state, J. Expt. Theor. Phys. **91**, 894 (2000).
[16] D. Gottesman and I. L. Chuang, Demonstrating the viability of universal quantum computation using teleportation and single-qubit operations, Nature (London) **402**, 390 (1999).
[17] M. Hillery, V. Bužek, and A. Berthiaume, Quantum secret sharing, Phys. Rev. A **59**, 1829 (1999).
[18] E. Guerra, Realization of GHZ states and the GHZ test via cavity QED, J. Mod. Opt. **52**, 1275 (2005).
[19] C.-L. Zhang, W.-Z. Li, and M.-F. Chen, Generation of W state and GHZ state of multiple atomic ensembles via a single atom in a nonresonant cavity, Opt. Commun. **312**, 269 (2014).

[20] M. Izadyari, M. Saadati-Niari, R. Khadem-Hosseini, and M. Amniat-Talab, Creation of *n*-atom GHZ state in atom-cavity-fiber system by multi-state adiabatic passage, Opt. Quantum Electron. **48**, 71 (2016).

[21] S.-B. Zheng, One-Step Synthesis of Multiatom Greenberger-Horne-Zeilinger States, Phys. Rev. Lett. **87**, 230404 (2001).

[22] Z.-H. Chen, P. Pei, F.-Y. Zhang, and H.-S. Song, One-step preparation of three-particle Greenberger-Horne-Zeilinger states in cavity quantum electrodynamics, JOSA B **29**, 1744 (2012).

[23] X. Zhang, Y.-H. Chen, Z.-C. Shi, W.-J. Shan, J. Song, and Y. Xia, Generation of three-qubit Greenberger-Horne-Zeilinger states of superconducting qubits by using dressed states, Quantum Inf. Proc. **16**, 309 (2017).

[24] T. Monz, P. Schindler, J. T. Barreiro, M. Chwalla, D. Nigg, W. A. Coish, M. Harlander, W. Hänsel, M. Hennrich, and R. Blatt, 14-Qubit Entanglement: Creation and Coherence, Phys. Rev. Lett. **106**, 130506 (2011).

[25] N. Friis, O. Marty, C. Maier, C. Hempel, M. Holzäpfel, P. Jurcevic, M. B. Plenio, M. Huber, C. Roos, R. Blatt *et al.*, Observation of Entangled States of a Fully Controlled 20-Qubit System, Phys. Rev. X **8**, 021012 (2018).

[26] A. Omran, H. Levine, A. Keesling, G. Semeghini, T. T. Wang, S. Ebadi, H. Bernien, A. S. Zibrov, H. Pichler, S. Choi *et al.*, Generation and manipulation of Schrödinger cat states in Rydberg atom arrays, Science **365**, 570 (2019).

[27] C. Song, K. Xu, H. Li, Y. Zhang, X. Zhang, W. Liu, Q. Guo, Z. Wang, W. Ren, J. Hao *et al.*, Observation of multi-component atomic Schrödinger cat states of up to 20 qubits, Science **365**, 574 (2019).

[28] X.-L. Wang, L.-K. Chen, W. Li, H.-L. Huang, C. Liu, C. Chen, Y.-H. Luo, Z.-E. Su, D. Wu, Z.-D. Li *et al.*, Experimental Ten-Photon Entanglement, Phys. Rev. Lett. **117**, 210502 (2016).

[29] H.-S. Zhong, Y. Li, W. Li, L.-C. Peng, Z.-E. Su, Y. Hu, Y.-M. He, X. Ding, W. Zhang, H. Li *et al.*, 12-Photon Entanglement and Scalable Scattershot Boson Sampling with Optimal Entangled-Photon Pairs from Parametric Down-Conversion, Phys. Rev. Lett. **121**, 250505 (2018).

[30] X.-L. Wang, Y.-H. Luo, H.-L. Huang, M.-C. Chen, Z.-E. Su, C. Liu, C. Chen, W. Li, Y.-Q. Fang, X. Jiang *et al.*, 18-Qubit Entanglement with Six Photons' Three Degrees of Freedom, Phys. Rev. Lett. **120**, 260502 (2018).

[31] J. P. Dowling, Quantum optical metrology—The lowdown on high-NOON states, Contemp. Phys. **49**, 125 (2008).

[32] K. T. Kapale and J. P. Dowling, Bootstrapping Approach for Generating Maximally Path-Entangled Photon States, Phys. Rev. Lett. **99**, 053602 (2007).

[33] M. W. Mitchell, Metrology with entangled states, in *Quantum Communications and Quantum Imaging III*, edited by R. E. Meyers and Y. Shih, Vol. 5893 (SPIE, 2005), pp. 263–272.

[34] P. Kok, H. Lee, and J. P. Dowling, Creation of large-photon-number path entanglement conditioned on photodetection, Phys. Rev. A **65**, 052104 (2002).

[35] G. J. Pryde and A. G. White, Creation of maximally entangled photon-number states using optical fiber multiports, Phys. Rev. A **68**, 052315 (2003).

[36] K. C. Cox, G. P. Greve, J. M. Weiner, and J. K. Thompson, Deterministic Squeezed States with Collective Measurements and Feedback, Phys. Rev. Lett. **116**, 093602 (2016).

[37] M. H. Schleier-Smith, I. D. Leroux, and V. Vuletić, States of an Ensemble of Two-Level Atoms with Reduced Quantum Uncertainty, Phys. Rev. Lett. **104**, 073604 (2010).

[38] S. Welte, B. Hacker, S. Daiss, S. Ritter, and G. Rempe, Cavity Carving of Atomic Bell States, Phys. Rev. Lett. **118**, 210503 (2017).

[39] F. Haas, J. Volz, R. Gehr, J. Reichel, and J. Estève, Entangled states of more than 40 atoms in an optical fiber cavity, Science **344**, 180 (2014).

[40] E. J. Davis, Z. Wang, A. H. Safavi-Naeini, and M. H. Schleier-Smith, Painting Nonclassical States of Spin or Motion with Shaped Single Photons, Phys. Rev. Lett. **121**, 123602 (2018).

[41] R. McConnell, H. Zhang, J. Hu, S. Ćuk, and V. Vuletić, Entanglement with negative Wigner function of almost 3000 atoms heralded by one photon, Nature (London) **519**, 439 (2015).

[42] M. A. Nielsen, Quantum computation by measurement and quantum memory, Phys. Lett. A **308**, 96 (2003).

[43] Y. Yan, Z. Jian, W. Lu, X. Bao-Ming, W. Chao-Quan, and S. Bin, Quantum state preparation and protection by measurement-based feedback control against decoherence, Commun. Theor. Phys. **63**, 149 (2015).

[44] R. H. Dicke, Coherence in spontaneous radiation processes, Phys. Rev. **93**, 99 (1954).

[45] M. Kitagawa and M. Ueda, Squeezed spin states, Phys. Rev. A **47**, 5138 (1993).

[46] H. Uys, M. Biercuk, J. Britton, and J. J. Bollinger, Toward spin squeezing with trapped ions, in *AIP Conference Proceedings*, edited by E. Brüning, T. Konrad, and F. Petruccione, Vol. 1469 (AIP, Umhlanga, SA, 2012), pp. 108–121.

[47] J. Hu, W. Chen, Z. Vendeiro, A. Urvoy, B. Braverman, and V. Vuletić, Vacuum spin squeezing, Phys. Rev. A **96**, 050301(R) (2017).

[48] W. Muessel, H. Strobel, D. Linnemann, D. B. Hume, and M. K. Oberthaler, Scalable Spin Squeezing for Quantum-Enhanced Magnetometry with Bose-Einstein Condensates, Phys. Rev. Lett. **113**, 103004 (2014).

[49] C. Lee, Q representation of the atomic coherent states and the origin of fluctuations in superfluorescence, Phys. Rev. A **30**, 3308 (1984).

[50] K. Jacobs, *Quantum Measurement Theory and its Applications* (Cambridge University Press, Cambridge, 2014).

[51] W. R. Gilks, S. Richardson, and D. J. Spiegelhalter, Introducing Markov Chain Monte Carlo, Markov Chain Monte Carlo in Practice **1**, 19 (1996).

[52] C. Sherlock, P. Fearnhead, G. O. Roberts *et al.*, The random walk metropolis: Linking theory and practice through a case study, Stat. Sci. **25**, 172 (2010).